International Journal of Mechanical Sciences 249 (2023) 108280

Contents lists available at ScienceDirect

International Journal of Mechanical Sciences

journal homepage: www.elsevier.com/locate/ijmecsci

Superbiphilic patterned nanowires with wicking for enhanced pool boiling heat transfer

Dong Il Shim [a], Wei-Ting Hsu [b], Maroosol Yun [a], Dongwhi Lee [c], Beom Seok Kim [d], Hyung Hee Cho [a,*]

[a] Department of Mechanical Engineering, Yonsei University, 50 Yonsei-ro, Seodaemun-gu, Seoul 03722, Republic of Korea
[b] Department of Nuclear Engineering, University of Tennessee, 2641 Osprey vista way, Knoxville TN 37920-4395, United States
[c] Department of Mechanical System Engineering, Jeonbuk National University, 567 Baekje-daero, Deokjin-gu, Jeonju-si, Jeollabuk-do 54896, Republic of Korea
[d] Department of Mechanical and Automotive Engineering, Seoul National University of Science and Technology, Seoul 01811, Republic of Korea

ARTICLE INFO

Keywords:
Boiling heat transfer
Surface modification
Superbiphilic
Surface wettability
Surface wicking
Critical heat flux

ABSTRACT

The boiling performance, represented by the heat transfer coefficient (HTC) and critical heat flux (CHF), must be enhanced because the energy demand of industrial processes that generate a lot of heat increases under extreme conditions. Surface manipulations have been used to improve boiling performance by controlling interfacial characteristics. Specifically, biphilic or superbiphilic patterned surfaces have been widely utilized to enhance HTC and CHF. However, it remains a challenging issue to improve CHF on superbiphilic surfaces with wicking phenomena due to the suppression of liquid supply in hydrophobic regions. In the present work, to investigate the mechanism and experimentally break through the limits of CHF enhancement, artificially patterned superbiphilic (SBPI) surfaces with different superhydrophobic (SHPO) area fractions were produced, and conducted pool boiling heat transfer. By artificially promoting nucleation, all SBPI surfaces demonstrated a higher HTC than homogeneous wettability surfaces. Considering dynamic wicking and bubble behaviors, the SBPI successfully broke through the CHF of homogeneous superhydrophilic surfaces. It is concluded that the non-dimensional liquid supply factor, which reflects both wicking and bubble behaviors, is essential to design structured surfaces during boiling. The results can contribute to a strategy for further improving boiling performance by controlling wettability on nanoscale interfaces.

1. Introduction

High-heat-generating energy systems must implement efficient thermal management to guarantee their performance and safety. Boiling heat transfer is one of the intensive cooling mechanisms for heat dissipation, removing thermal energy through phase change phenomena of working fluid with a stable surface temperature of a device [1–4]. Consequently, it has been utilized for thermally sensitive systems with high thermal loads, such as power generating systems, and immersion cooling of integrated electronic devices [5–7]. Many studies have been widely conducted to improve boiling performance because various industrial fields require extremely high-efficiency heat transfer [8–14]. Increasing heat transfer efficiency and ensuring thermal stability under extreme conditions are the two primary approaches to enhancing boiling performance. The heat transfer coefficient (HTC), the ratio of input heat flux to wall superheat, was proposed to evaluate heat transfer efficiency. The critical heat flux (CHF) is another major factor in determining boiling performance. CHF is the limiting point of fully developed nucleate boiling before forming a vapor film. When the thermal load reaches the CHF, a vapor film blocks the coolant supply to the heated surface; the low thermal conductivity of the vapor layer may cause thermal damage. Hence, simultaneous enhancement of the HTC and CHF should be achieved for effective thermal management and safety of the system.

Surface manipulation is an effective method to improve boiling performance via manipulating interfacial characteristics and consequent nucleation behaviors [15,16]. Surface wettability is the representative interfacial property of engineered surfaces closely related to CHF. Particularly, hydrophilicity improves the supply of working fluid to the boiling surface and delays the formation of vapor film to increase the CHF. In addition, the wicking coefficient, the rate of liquid propagation between structured surfaces with capillary effects, was used to evaluate the dynamic wetting characteristics. High-wicking ability has further

* Corresponding author.
E-mail address: hhcho@yonsei.ac.kr (H.H. Cho).

https://doi.org/10.1016/j.ijmecsci.2023.108280
Received 28 November 2022; Received in revised form 28 February 2023; Accepted 6 March 2023
Available online 7 March 2023

Nomenclature

Symbols

A_b	cross-sectional area of single bubble (mm^2)
A_{wick}	wicking area (mm^2)
A_{total}	total area (mm^2)
d	diameter of superhydrophobic dots (mm)
D_b	bubble departure diameter (mm)
h	height of nanowires (μm)
h_{lv}	latent heat of liquid-vapor phase (J/g)
p	pitch of superhydrophobic dots (mm)
P_b	perimeter of single bubble (mm)
$q''_{add,\ wick}$	additional heat dissipation caused by the evaporation of wicked liquid (W/cm^2)
$q''_{CHF,\ plain}$	critical heat flux on silicon plain (W/cm^2)
r	surface roughness factor
W	wicking rate ($mm/s^{0.5}$)
$W_{eff,V}$	effective volumetric wicking rate (mm^3/s)

Greek symbols

θ	Young's contact angle ()
θ*	apparent contact angle ()
θ_c	critical contact angle ()
λ_c	critical wavelength (mm)
ρ_l	density of liquid (g/mm^3)
φ	solid fraction

Abbreviation

CHF	critical heat flux
FE-SEM	field emission scanning electron microscope
FOTS	fluoro-octyltrichloro silane
H-SHPI	homogeneous superhydrophilic
H-SHPO	homogeneous superhydrophobic
HTC	heat transfer coefficient
MACE	metal-assisted chemical etching
ONB	onset of nucleate boiling
SBPI	superbiphilic
SEM	scanning electron microscope
SHPI	superhydrophilic
SHPO	superhydrophobic
SiNWs	silicon nanowires

enhanced CHF through additional heat dissipation by immediately supplying liquid to the local dry areas. Recently, various manipulated surfaces accompanied by wicking have been applied for enhanced boiling, and new CHF enhancement models have been proposed. Ahn et al. [17] provided liquid spreading models to explain CHF enhancement on nanostructured surfaces. The volume of liquid spread was evaluated by the volume difference between the initial and remained droplet. Kim et al. [18] used aligned nanopillars with different diameters to analyze the mechanism of CHF enhancement. Wicking distance could be measured using high-speed wicking propagation images, and the wicking coefficient was calculated by the ratio of wicking distance to the square root of time. Rahman et al. [19] described that additional heat dissipation by wicked liquid based on calculated wicked volume flux. Song et al. [20] investigated the wicking speed of various sandblasted surfaces, and described CHF enhancement using a unified descriptor considering both surface roughness and wicking speed. In early research to predict CHF, the correlations were provided considering the hydrodynamic instability [21–23], wettability [24], and roughness [25,26]. In the case of the surface with wicking phenomena, generally, the CHF can be described as the sum of the conventionally derived hydraulic model and the additional heat dissipation capacity provided by wicking.

Bubble departure characteristics, closely related to the HTC, are also important factors in boiling performance [27]. Early onset of nucleate boiling (ONB) facilitates developing two-phase heat transfer to a broad area with enhanced micro scale convection, evaporation, and quenching mechanisms during boiling. Hence, research on surface manipulations was conducted to promote the ONB and control nucleate site density on various engineered surfaces such as nanowires [28], channels [29], micro-cavity [30], reentrant structures [31], and micro-nano hybrid structures [32,33]. The bubble behaviors also had a significant effect on the CHF because it was directly involved in vapor film formation. Several studies have achieved CHF improvement by effectively separating liquid-vapor pathway using porous structures [34,35], honeycomb plate [36], 3d-printed composite porous structure [37], 3d-printed polymer structures [38].

Recently, novel methods to obtain the early onset of nucleation and separating liquid-vapor pathway have been implemented using the biphilic surface (i.e., heterogenous wettability surface). The objective of biphilic surface was to accomplish the synergetic effect of the heterogeneous wettability surfaces to promote nucleation activation on the hydrophobic and ensure the liquid supply on the hydrophilic regions, respectively. Betz et al., [39] applied biphilic surfaces to improve boiling heat transfer, and successfully demonstrated that CHF and HTC could be enhanced using hydrophilic networks with hydrophobic islands. Jo et al., [40,41] demonstrated meaningful results that boiling heat transfer improvement on biphilic patterned surfaces by analyzing bubble motions. Shen et al. [42] explained the early ONB and enhanced HTC on biphilic surfaces by experiments and simulations of bubble behaviors. Hsu et al. [43] conducted flow boiling utilizing different shapes and parameters of biphilic patterns. Zhang et al. [44] fabricated the 3D heterogeneous wetting microchannels and evaluated the boiling performance. Ateş et al. [45] investigated the boiling performance on superbiphilic surfaces at atmospheric and sub-atmospheric pressures. Recently, efforts to maximize boiling performance have been actively reported using optimum parametric design or nanoscale textured superbiphilic characteristics [46–49]. The boiling experiments using the biphilic surfaces demonstrated that the HTC is enhanced by the early ONB, the starting point of the boiling mechanism; hydrophobic patterns regulate nucleate sites and increase the density of activated nucleation for enhanced HTC. Moreover, the bubble departure diameter has changed due to a strong pinning effect at the hydrophilicity-hydrophobicity boundaries [50,51]. Compared to bare surfaces or homogeneous wettability surfaces, controlled nucleate sites on biphilic surfaces have increased the CHF by separating the liquid supply and vapor departure regions. Several studies have applied superbiphilic (SBPI) surfaces, which employ nanostructured surfaces accompanied by wicking phenomena, to improve boiling performance [52,53]. Table A.1 in Appendix A of supporting information (SI) briefly summarizes the materials and boiling heat transfer results in previous works. Remarkably, the HTC has increased significantly on the SBPI surfaces due to superhydrophobicity which has stimulated bubble nucleation and maximized nucleate density. However, the CHF did not exhibit the expected improvement; rather, it decreased compared to the homogeneous superhydrophilic (SHPI) surface. The superhydrophobic (SHPO) dots significantly impact the deterioration of liquid propagation capabilities on wicking surfaces. Therefore, due to the wicking area reduction effects, the CHF decreases as the hydrophobic area fraction increases. Therefore, it remained a challenging task to improve CHF as well as maximize HTC on superbiphilic surfaces with wicking.

This study proposes strategically controlled SBPI patterns on wicking surfaces to improve HTC and CHF simultaneously during pool boiling heat transfer. The 5 μm-high silicon nanowires (SiNWs) were fabricated

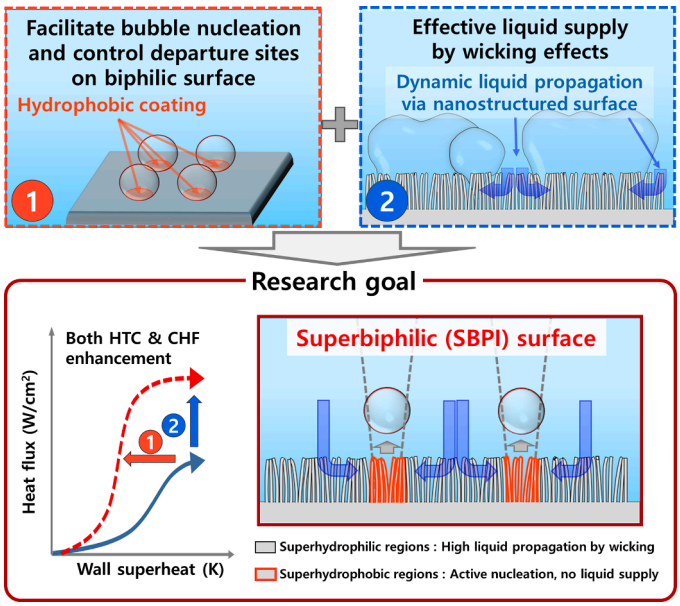

Fig. 1. Strategy for enhanced heat transfer coefficient (HTC) and critical heat flux (CHF) simultaneously using SBPI surface. Hydrophobic coating promotes bubble nucleation to improve HTC, and wicking phenomena on nanowires enhance CHF. The SBPI surface utilizes the synergetic effect of superhydrophobicity and superhydrophilicity to enhance boiling performance.

to obtain the SHPI base surface, which has wicking phenomena. As the primary design parameter, the SHPO area fraction is controlled by three different diameters of low surface energy-coated dots. Fig. 1 depicts the anticipated boiling performance enhancement mechanism. The superhydrophobicity will aid in nucleation from low heat flux. Active bubble departure behavior with a high nucleation site density contributes to efficient heat dissipation. High heat flux dissipation requires the maintenance of superhydrophilicity and wicking properties to supply coolant effectively. We demonstrate through experimental evaluations that a SBPI surface with less than 1% -SHPO area fraction is adequate for retaining a high liquid supply via minimal liquid propagation obstruction. Pool boiling experiments and visualization of bubble departure characteristics were conducted to validate the SBPI surfaces' strategy for enhancing boiling performance.

2. Materials and methods

This section demonstrates the specimen preparations and details of the experimental equipment. First of all, the wettability-controlled surface or SBPI surfaces fabrication processes based on the theoretical approaches are provided. Also, the parametric design of nanowire arrays and SHPO dot islands are described. The methods to evaluate interfacial properties are explained by containing wettability, morphology, and bubble dynamics during boiling. Finally, the pool boiling experimental setup and data reduction process with uncertainties are discussed.

2.1. Fabrication of homogeneous super-wettabilty surface and SBPI patterns

Superhydrophilicity was achieved by fabricating SiNWs with high surface roughness. Superhydrophobicity was obtained by additional low surface free energy coating on SiNWs using fluoro-octyltrichloro silane (FOTS). Metal-assisted chemical etching (MACE) was performed to fabricate SiNWs [54]. Detailed fabrication processes of homogeneous wettability surfaces and SBPI surfaces are explained in SI. Due to the increased surface roughness and high surface free energy of intrinsic silicon, SiNWs exhibit SHPI properties. The apparent contact angle of rough surfaces can be described by Wenzel's model in hydrophilic surfaces as follows [55,56]:

$$cos\theta^* = rcos\theta \tag{1}$$

where θ* corresponds to the apparent contact angle, r denotes the surface roughness factor, and θ is Young's contact angle on the ideal plain surface. In Wenzel's model, the working fluid rapidly permeates and propagates between the structures. The hydrophilicity is strengthened by increasing the surface roughness; after that, the superhydrophilicity can be achieved by a high aspect ratio of SiNWs. Conversely, the working fluid does not penetrate between surface structures on the hydrophobic surfaces in Cassie-Baxter's model [56,57].

$$cos\theta^* = -1 + \varphi(cos\theta + 1) \tag{2}$$

where φ denotes the solid fraction, which is the ratio of solid contact area to the total area. Superhydrophobicity could be achieved by low surface energy coating and decreasing the solid fraction via nanostructures [56,58,59]. In the present work, FOTS was coated on the silicon surface to reduce surface energy for hydrophobicity.

Six surfaces having different wettability characteristics and SHPO patterned diameters were applied in pool boiling experiments. The boiling surfaces were separated into two major sections: surfaces with homogeneous wettability and SBPI. The former consisted of silicon (Si plain), SiNWs representing the homogeneous SHPI (H-SHPI) surface, and FOTS-coated SiNWs representing the homogeneous SHPO (H-SHPO) surface. The SBPI surfaces have circular FOTS patterned with various diameters ranging from 0.1 mm to 1.0 mm on SiNWs. On the SBPI surfaces, the diameter of patterns was controlled by photolithography using a positive photoresist (PR). Details of the fabrication process to obtain the SBPI surface are described in SI.

The surface characteristics, which include the contact angle, patterns dimensions, and SHPO area fraction (A_{SHPO}/A_{total}) are listed in Table 1. Remarkably, A_{SHPO}/A_{total} was only 0.26% on SBPI surface with a diameter of 0.1 mm (SBPI_d0.1). The SBPI_d0.1 could maintain the

Table 1
Geometric variables and consequent wetting characteristics on homogeneous wettability surfaces and SBPI surfaces.

Abbreviation	Homogeneous wettability surface			Superbiphilic (SBPI) surface		
	Base case	Homogeneous Superhydrophillic (H-SHPI)	Homogeneous Superhydrophobic (H-SHPO)	SBPI_d0.1	SBPI_d0.5	SBPI_1.0
Materials	Si plain	SiNWs	SiNWs+FOTS	SiNWs+Patterned FOTS	SiNWs+Patterned FOTS	SiNWs+Patterned FOTS
Height of SiNWs (*h*) (μm)	–	5	5	5	5	5
Number of patterns	–	–	–	49 (7 × 7)	49 (7 × 7)	49 (7 × 7)
Pattern pitch (p) (mm)				1.75	1.75	1.75
Pattern diameter (d) (mm)				0.1	0.5	1.0
Contact angle (°)	46	7	169	7, 169	7, 169	7, 169
A_{SHPO}/A_{total} (%)	0	0	100	0.26	6.41	25.65

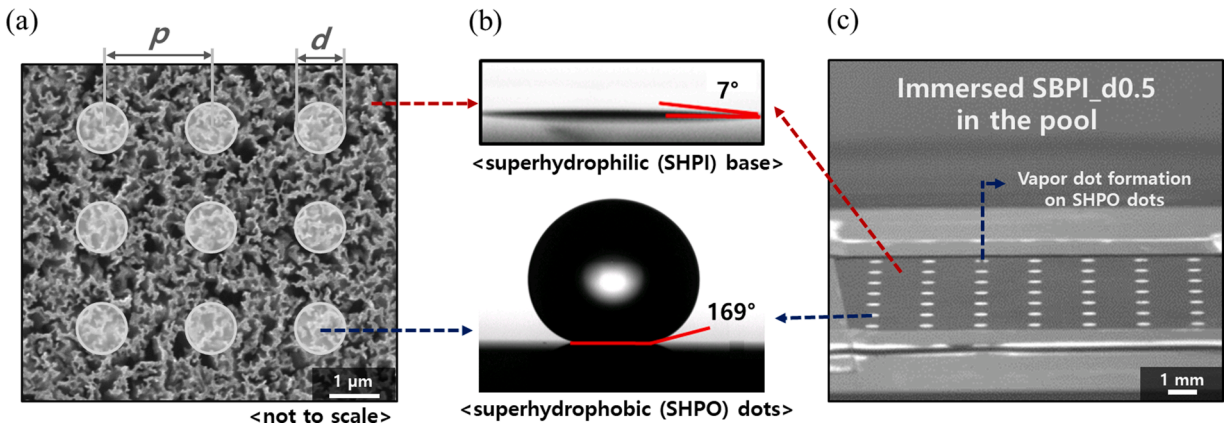

Fig. 2. SBPI surfaces fabricated by SiNWs and FOTS coating. (a) SEM image of SiNWs, and SHPO dot parameters on SBPI surfaces (scale bar only indicates for SEM image), (b) contact angle of SHPI regions and SHPO dot regions, and (c) immersed images of SBPI_d0.5 in the DI water pool are demonstrated.

superhydrophilicity and wicking property as much as possible compared to other SBPI cases by reducing the SHPO area. Fig. 2 shows the fabrication results of SBPI surface. Fig. 2(a) indicates the design parameters of SHPO patterns on SHPI surface to achieve SBPI surface. The contact angle of SHPO and SHPI regions are shown in Fig. 2(b). Fig. 2(c) is the immersed image of SBPI_d0.5 before heating. Especially, primary vapor dots were observed on the SHPO dots of SBPI surfaces.

2.2. Analysis on interfacial characteristics (morphology and wettability)

The surface morphology of SiNWs and FOTS coated SiNWs was analyzed using a field emission scanning electron microscope (FE-SEM, JEOL 7800F). Cross-sectional images were used to determine the height and pitch. The height of nanowires was fixed at 5 μm. According to our previous research, 5 μm-SiNWs are sufficient to provide surface roughness for superhydrophilicity accompanied by dynamic wicking phenomena [56,60]. In particular, the wicking coefficient of 5 μm -SiNWs has been measured to 0.4 mm/$s^{0.5}$ [61]. The static contact angles were investigated by a static sessile droplet method [56,62] using a contact angle goniometer (KSV, CAM-200). After dropping 2.5 μl of deionized (DI) water on each surface, the cross-sectional images were captured at 500 fps using a high-speed camera. The contact angle should be measured in three-phase equilibrium; however, on the SiNWs, the droplet was absorbed and propagated by wicking phenomena between the structures. As a result, the contact angle of SiNWs appears close to zero. Consequently, the angles were provided immediately after the droplet contacted the SiNWs. (Δt=0.01 s). As the superhydrophilicity and superhydrophobicity are not clearly defined, in the present work, it is expressed as superhydrophilic when the contact angle is lower than 10°, and superhydrophobic when the contact angle is larger than 150° [56,63,64].

During pool boiling experiments, bubble departure behaviors are dependent on surface conditions. The average bubble departure diameters were measured in present works. To analyze bubble characteristics, horizontal and 10° tilted images were recorded using a high speed camera (Speedsense M310, Dantec.). The qualitative investigations of nucleate sites and bubble coalescence phenomena on heated surfaces were evaluated by tilted images. The quantitative values of bubble departure diameter could be calculated using horizontal shadowgraph images with 100 W LED light source. The bubbles were assumed perfect circles, and a commercial program (Dynamic studio 5.1) calculated the bubble departure diameter (D_b) using the below equation [32].

$$D_b = 1.55 \cdot \frac{A_b^{0.625}}{P_b^{0.25}} \tag{3}$$

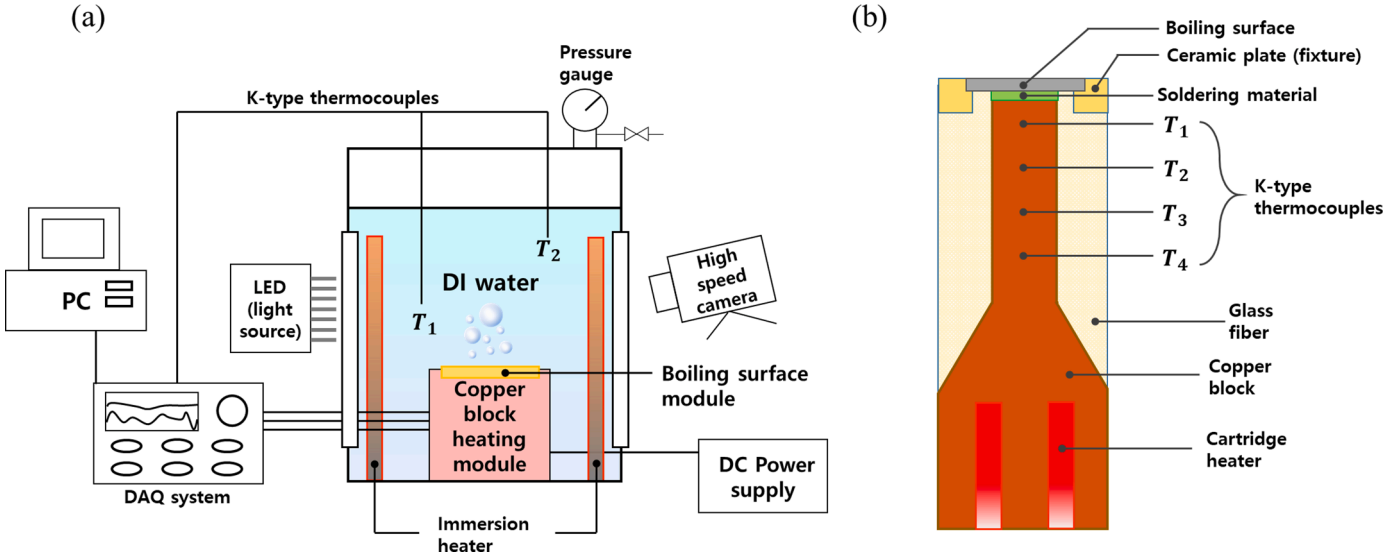

Fig. 3. Pool boiling experiment equipment; (a) Experimental setup for pool boiling experiment and (b) a schematic of thermally attached boiling surface module on the copper block heating module.

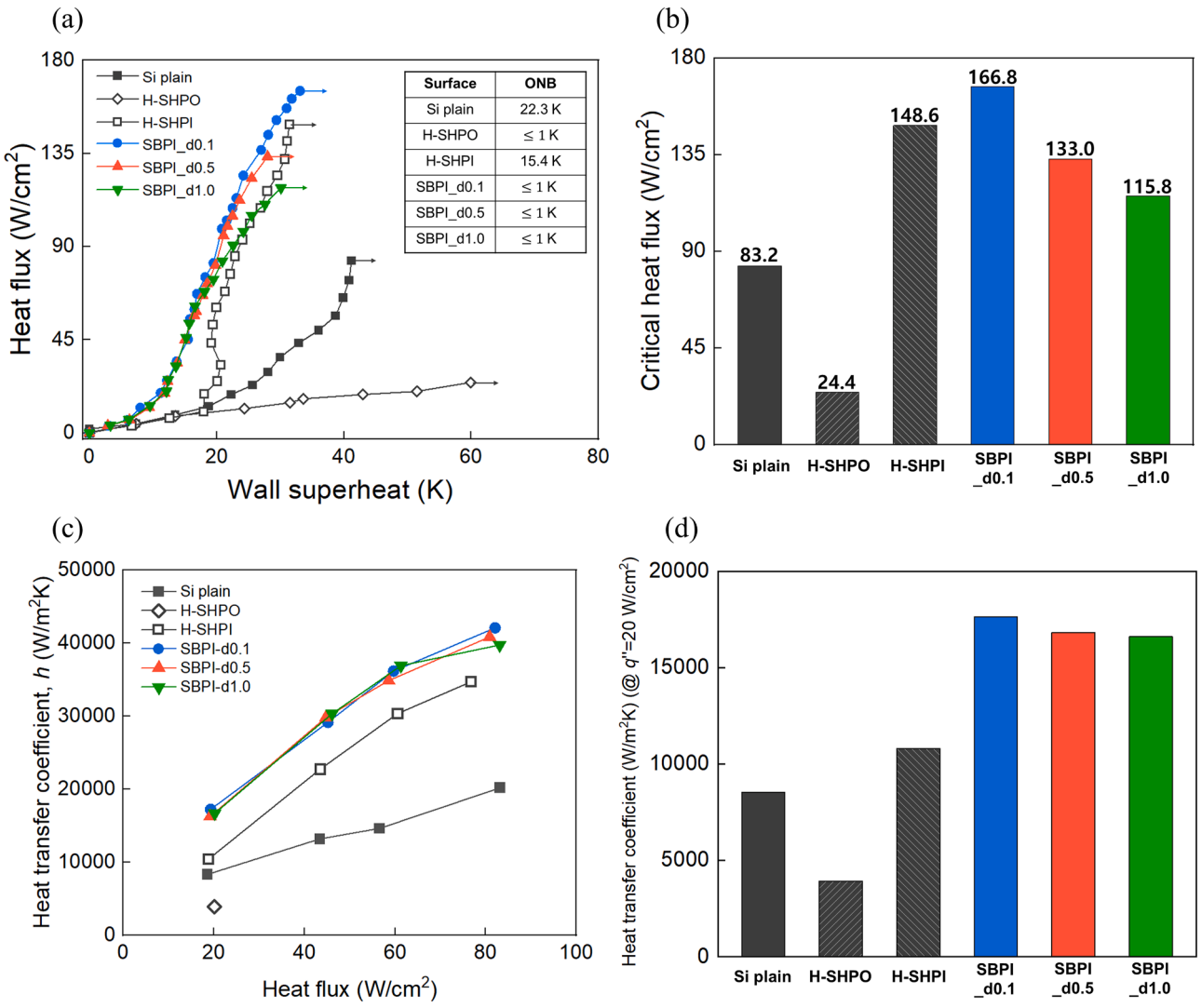

Fig. 4. Pool boiling experimental results; (a) boiling curves on 6 different surfaces which have homogeneous wettability or SBPI surfaces, (b) CHF values, (c) HTC during middle heat flux regions (20–80 W/cm^2), and (d) HTC values at 20 W/cm^2. ONB results of silicon plain and wettability-controlled surfaces were indicated in the inset table. Notably, nucleation occurred at less than 1 K on the surfaces with superhydrophobicity because it forms a pre-vapor film with immersed conditions. Early ONB with controlled nucleation sites on SBPI surfaces could enhance HTC effectively. As a result, HTC were improved on the SBPI surfaces compared to homogeneous wettability surface. However, CHF was only improved on the SBPI_d0.1 surface compared to H-SHPI surface by 12.2%.

where A_b and P_b represent the cross-sectional area and perimeter of single bubble, respectively. Also, in order to increase the precision of the diameter, the average value was calculated using three data points at two different nucleation sites on each boiling surface.

2.3. Pool boiling experiment

The pool boiling experiment was conducted using a copper block heater, as described in Fig. 3. The apparatus consisted of three main parts: the fluid chamber, copper block heating module, and boiling surface specimen. The fluid chamber was made of stainless steel with 200 × 200 × 200 mm^3. Each side wall contained transparent windows for observing the characteristics of bubble behavior. The deionized (DI) water was used as a working fluid. Four vertically-spaced immersion heaters were installed in the chamber's corner to maintain the saturation temperature of the working fluid via PID control. Two K-type thermocouples were used to measure the working fluid temperature during the pool boiling experiment.

The copper block heating module, which has a heated area of 10 × 10 mm^2, transfers heat flux to boiling surface specimens. A programmable power supply (SGI 200 × 25, AMETEK) supplied current to four cartridge heaters (150 V DC with 120 W of power) inserted in the copper block. To evaluate the 1-dimensional temperature gradient during boiling experiments, four K-type thermocouples were inserted at 7 mm intervals in the middle of a copper block neck. To minimize the lateral heat loss for securing 1-dimensional conduction approximation, copper block was thermal insulated by glass fiber except for upward direction which contacts the boiling surface. The boiling test chips, aforementioned in Section 2.1, were fixed on the boiling surface module and thermal contacted by soldering materials to the top of the copper block heating module. The boiling surface module was made of polyether ether ketone (PEEK) to minimize lateral heat loss due to its low thermal conductivity (~0.25 W/mK). Through repeated experiments, repeatability was confirmed to increase the reliability of the experimental results. Details of the data reduction process and the repeated experimental results on all cases are demonstrated in Appendix B of SI.

The uncertainties of parameters were evaluated using Moffat's approach [65]. The error of temperature by K-type thermocouple was 1.1 K. The lateral conduction heat loss of silicon chips was evaluated by commercial software (ANSYS, 6.3.26) [38,61]. Detailed analysis process of uncertainties and results are described in Appendix B of SI. As a result,

the maximum uncertainties of heat flux, wall superheat, and heat transfer coefficient were ± 6.6%, 7.0%, and 9.6%, respectively. The uncertainty of bubble departure diameter size caused by pixel was described in previous work [32], and the values were ± 0.1 mm.

3. Results and discussion

The boiling heat transfer experimental results are demonstrated in this section, and the CHF and HTC enhancement mechanism analyses are explored. Also, boiling results are compared with previous works using biphilic or superbiphilic patterned surfaces. Firstly, the boiling curves containing CHF and HTC values on each surface are provided. Then, the mechanism would be discussed with single/arranged bubble dynamics and wicking properties. Finally, new approaches using both micro and macro scale liquid supply are suggested to explain the results of present works and the potential for further improvements in future work.

3.1. Simultaneous enhancement of HTC and CHF on SBPI surface

The results of the pool boiling experiment are demonstrated in Fig. 4. Fig. 4(a) shows the input heat flux versus wall superheat and Fig. 4(b) shows the ratio of CHF compared to Si plain case. Fig. 4(c) shows the HTC during middle heat flux regions. In particular, Fig. 4(d) shows the ratio of HTC compared with Si plain case at 20 W/cm^2. As shown in the inset table of Fig. 4(a), ONB of H-SHPO and all SBPI cases occur at extremely lower wall temperatures (under 1 K) than ONB of Si plain (22.3 K) and H-SHPI (15.4 K). These results indicate that bubble nucleation could be activated through the superhydrophobicity and only occur at SHPO islands. The CHF on the plain Si surface representing the base case was 83.2 W/cm^2. On the H-SHPI, the CHF increased by 78.6% (148.6 W/cm^2), while on the H-SHPO surface, it decreased by 70.7% (24.4 W/cm^2). Among the homogeneous wettability surfaces (shown in gray), the H-SHPI surface revealed an enhancement in heat flux dissipation with relatively low wall superheat compared to the H-SHPO surface. Our previous research and other published works have demonstrated that CHF can be enhanced by supplying additional working fluid to local dry regions via structured surfaces accompanied by wicking phenomena [17,18,66]. Wicking occurs when the apparent contact angle is less than the critical contact angle (θ_c), which is derived based on the variation of surface energy as follows [18,61]:

$$\theta_c = \cos^{-1}\left(\frac{1-\varphi}{r-\varphi}\right) \tag{4}$$

where r denotes the surface roughness factor and φ denotes the solid fraction. Each parameter was calculated assuming a rectangular arrangement and was defined as $r \equiv 1 + \pi dh/p^2$ and $\varphi \equiv \pi d^2/4p^2$. The critical contact angle of 5-μm high SiNWs was approximately 89°, which was sufficient to meet wicking criteria. Consequently, the additional liquid supply by wicking on the H-SHPI surface enhanced micro scale evaporation and quenching at local dry spots, increasing CHF. In addition, compared to Si plain, the surface morphology of SiNWs favors the bubble nucleation, allowing bubbles to depart with small size (accelerating the departure frequency) and thereby improving the HTC [67,68]. In contrast, the CHF and HTC diminished significantly on the H-SHPO surface. These results can be explained by the behavior of vapor growth, as shown in Figure C.1 in Appendix C of SI. The bubble grew in the lateral direction while maintaining the contact angle. Even at low heat flux, a vapor film was formed over the entire H-SHPO surface with a large contact angle between the solid and liquid interface. Vapors grew by interfacial evaporation on a boiling surface, and the vapor film rose vertically due to buoyancy. Moreover, the bubble was desorbed from the middle of the vapor column by the necking effect, and the surface was continuously covered with a residual vapor film during boiling. The residual film blocked rewetting for quenching and evaporation on the heated surface. Therefore, the boiling performance, represented by the CHF and HTC, extremely deteriorated on the H-SHPO due to being cooled by only natural convection with the low thermal conductivity of the vapor film.

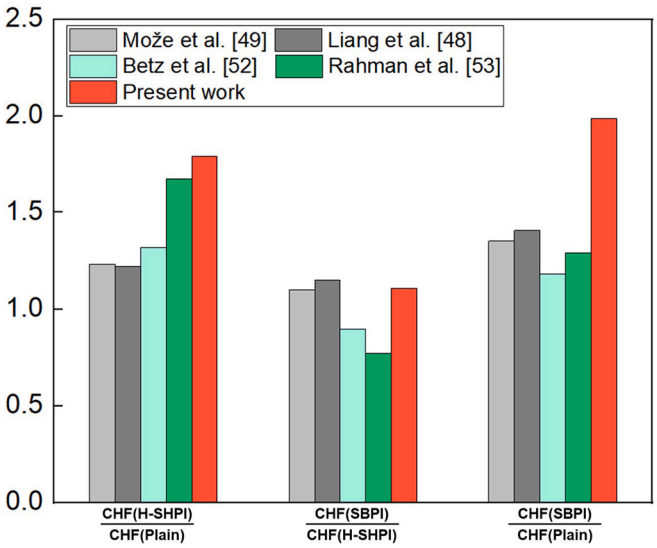

Fig. 5. CHF enhancement ratio using superbiphilic surface reported in previous research and present work. Betz et al. [52] and Rahman et al. [53] demonstrated CHF reduction on SBPI surface compared with H-SHPI due to suppression of wicking phenomena. In this study, we overcome the limitation of CHF enhancement approach using both wickability and biphilic patterns. Therefore, CHF ratio of SBPI surface to plain surface has the highest value among the research using superbiphilic surfaces.

The experimental results of the SBPI surfaces were obtained on the three different diameters of the patterns (plotted in color). The HTC of all SBPI cases were improved at the same heat flux compared with the homogeneous wettability surfaces (i.e. boiling curves are shifted to left). These results indicate that a relatively high heat flux can be dissipated even at a low surface wall superheat using SBPI surface. The nucleate site density increased from the low heat flux region by artificially manipulating and promoting the bubble nuclei points. The nucleation promotion effects on SHPO regions were experimentally verified by ONB evaluations as mentioned above. As a result, HTC was improved in the entire boiling region, which is consistent with the results of the study on boiling heat transfer using biphilic or SBPI surfaces [39,52]. CHFs were increased compared to the Si plain surface by 100.4% (166.8 W/cm^2), 59.9% (133.0 W/cm^2), and 39.2% (115.8 W/cm^2) on the SBPI_d0.1, SBPI_d0.5, and SBPI_d1.0 surfaces, respectively. These results demonstrate that the SHPO area fraction on SBPI is one of the key factors in boosting CHF by liquid supply to a local dry area.

Fig. 5 demonstrates the CHF enhancement ratio using superbiphilic patterned surfaces in previously reported studies and present work. Although all surfaces showed superhydrophilic properties, the value of 'CHF(H-SHPI)/CHF(Plain)' improved according to the presence of wicking and performance improvement. However, SBPI surface with wicking [52,53] had less than 1 of 'CHF(SBPI)/CHF(H-SHPI)' due to the reduction of SHPI and wicking area. On the other hand, in the present work, the SBPI surface had a larger CHF than H-SHPI. Therefore, both high wickability and additional CHF enhancement by superbiphilic patterns could enhance effectively. Then, 'CHF(SBPI)/CHF(Plain)' had the highest values on the present work among utilizing superbiphilic surfaces.

Particularly, an additional increase in the CHF was observed on the SBPI_d0.1 surface compared to the H-SHPI surface. Using that particular SBPI surface, both HTC and CHF were improved simultaneously. It means that the wicking property is not the only factor determining CHF during boiling heat transfer. In this regard, bubble departure site

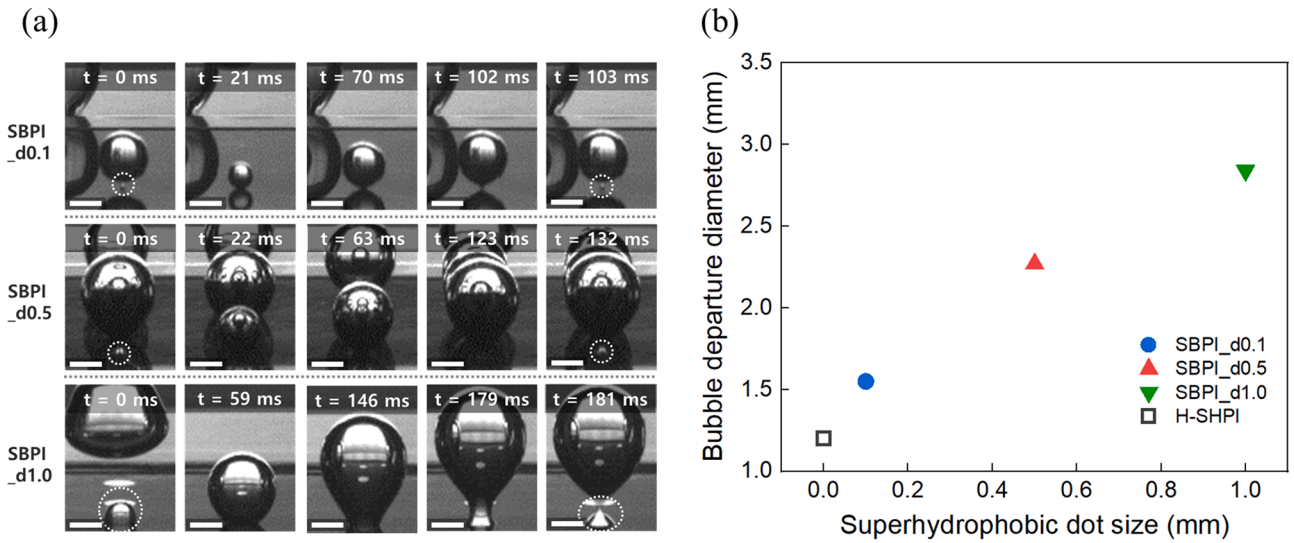

Fig. 6. (a) Bubble growth and departure characteristics on the SBPI surfaces. The scale bar indicates 1 mm. (b) Average bubble departure diameter versus SHPO dot sizes. As SHPO dot size increases, the bubble departure diameters were enlarged.

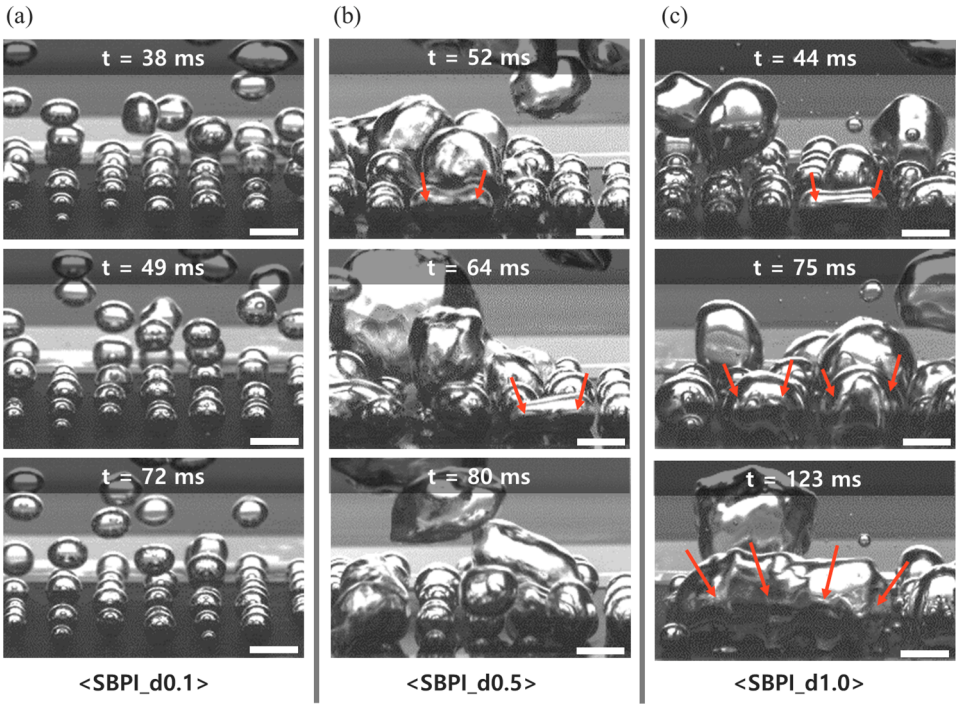

Fig. 7. Bubble departure images with the interaction between adjacent bubbles on (a) SBPI_d0.1, (b) SBPI_d0.5, and (c) SBPI_d1.0, respectively. The red arrows indicate bubble coalescence during bubble growth. Significantly, bubbles were detached independently on the SBPI_d0.1 surface which has a larger pitch between SHPO dots than single bubble size.

arrangement is conjectured as another underlying mechanism in the CHF enhancement. To demonstrate this speculation, the bubble departure characteristics were investigated.

3.2. Bubble departure and liquid supply characteristics on SBPI surfaces

The bubble departure characteristics were analyzed to comprehend the boiling performance enhancement mechanism on SBPI surfaces. Fig. 6(a) demonstrates the growth and departure of a single bubble on SBPI surfaces. The bubble was nucleated on the SHPO dot and grew along the SHPO dot-SHPI area contact line. The bubble grew in the lateral direction, maintaining the contact angle on SHPO region. However, this lateral expansion of bubbles was blocked, and the contact angle was changed into the hydrophilic region by a strong pinning effect. Eventually, the bubble grew spherically and detached from SHPO dots. Therefore, there is a close relationship between the bubble departure diameter and the SHPO dot size. Fig. 6(b) demonstrates the average bubble departure diameter on the SBPI surfaces and H-SHPI surfaces. On the SBPI_d0.1 surface, the pinning effect produced a sharp bubble departure angle, which is favorable for liquid supply. Furthermore, the interfacial tension on the boundary contact line was relatively low on the smaller SHPO dot size due to the reduced perimeter.

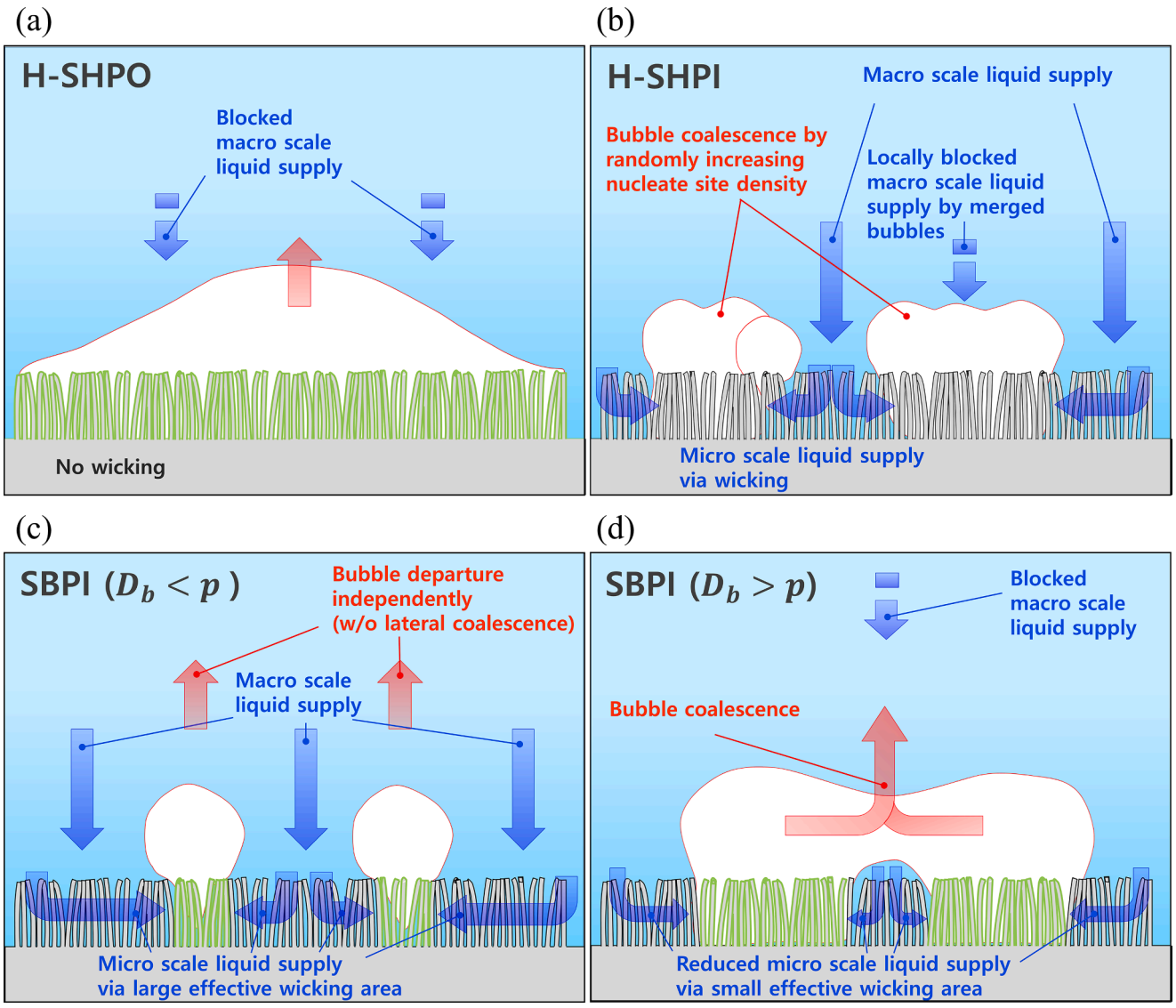

Fig. 8. The schematic of macro scale and micro scale liquid supply to heated surface on (a) H-SHPO, (b) H-SHPI, (c) SBPI surface ($D_b < p$), and (d) SBPI surface ($D_b > p$). During boiling heat transfer, the SBPI surface ($D_b < p$) has an advantage for improving both macro and micro scale liquid supply.

Consequently, a bubble could easily separate from the surface during bubble growth. Therefore, the average diameter of departed bubbles on the SBPI_d0.1 surface was approximately 1.55 mm. On the SBPI_d1.0 surfaces, however, the bubbles grew vertically and were separated by the necking effect. These bubble departure characteristics impede working fluid supply because of liquid blockage around the vapor column. The bubble grew to ensure enough buoyancy force to be detached from the surface resisting interfacial tension; hence, the relatively large departure diameters of 2.27 mm and 2.84 mm were obtained on SBPI_d0.5 and SBPI_d1.0, respectively.

To further quantify the bubble interaction between adjacent hydrophobic dots, bubble departure behaviors on the overall SBPI areas were analyzed when the heat flux was 50 W/cm^2, as shown in Fig. 7. In common on the three SBPI surfaces, early bubble formation was observed on all SHPO dots of the test substrates. Effective micro convection and evaporation via bubble departure were accomplished by artificially increasing the nucleate site density from an extremely low heat flux; consequently, HTC can be improved on the SBPI surfaces. The different behaviors of bubble coalescence appeared on each SBPI surface due to a ratio between the single bubble departure diameter and the pitch of SHPO dot patterns. During bubble growth on the SBPI_d0.5 and SBPI_d1.0 surfaces, lateral coalescence occurred because the bubble size was greater than the pitch of nucleate sites. This coalescence reduces the liquid supply to the heated surfaces by obstructing the liquid supply pathway. Additionally, lateral bubble coalescence raises the probability of developing into vapor film formation. On the SBPI_d0.1 surface, however, the bubbles departed independently. In this study, the pitch of SHPO dots was maintained at 1.75 mm, which was sufficient to prevent bubble merging due to the smaller bubble departure diameter on the SBPI_d0.1 surface. Therefore, the macro scale liquid was supplied to the boiling surface without disturbance by the merged bubbles.

Fig. 8 shows the bubble departure and liquid supply characteristics on homogeneous wettability and SBPI surfaces based on experimental results. The H-SHPO surface forms a vapor film and blocks both macro and micro scale liquid supply. On the other hand, micro scale liquid supply via wicking occurs on the H-SHPI surface; however, as heat flux increases, the random formation of nucleate sites raises the probability of local vapor film formation. Fig. 8(c) and 8(d) demonstrate the liquid supply mechanism on the SBPI surfaces. As the SHPO dot size decreases, the effective wicking area increases, enhancing the micro scale liquid supply capabilities. On the SBPI surface which has a smaller bubble departure diameter than the pitch between adjacent bubbles, macro scale liquid supply can be ensured by separating the liquid and bubble pathway. In Section 3.3, the relationship between liquid supply abilities

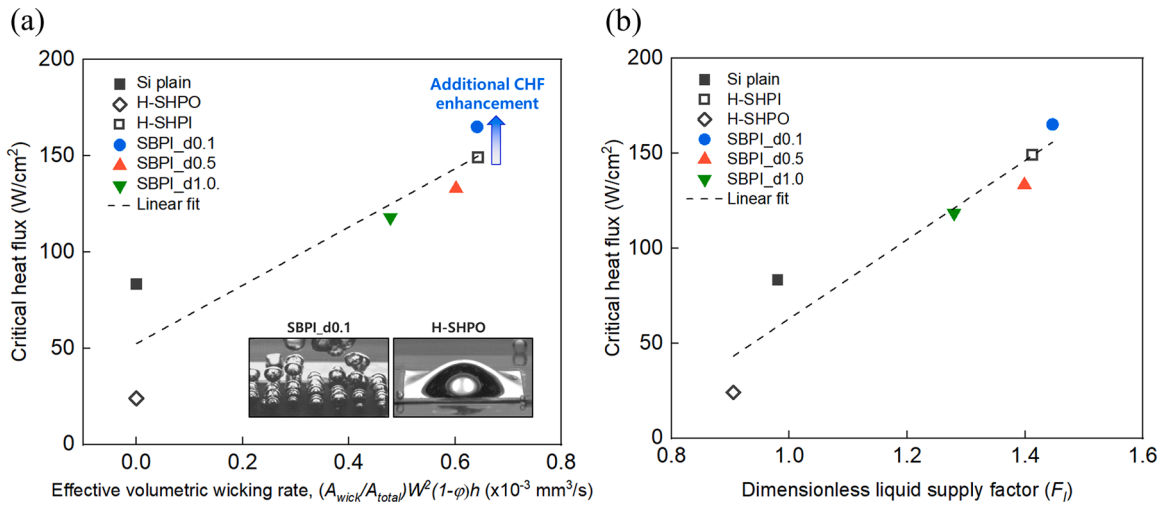

Fig. 9. (a) CHF vs effective volumetric wicking rate: the wicking phenomenon is insufficient to fully explain the CHF on wettability-controlled surfaces. H-SHPO surface has a smaller CHF compared to Si plain, and SBPI_d0.1 has a larger CHF compared to H-SHPI surface although it has a lower effective volumetric wicking rate. (b) CHF vs dimensionless liquid supply factor: considering both macro and micro scale liquid supply on wettability-controlled surfaces, it clearly demonstrates that the CHF can be enhanced by improving bubble behaviors and wicking properties.

and CHF on SBPI surfaces are discussed.

3.3. Enhanced CHF by ensuring quick liquid supply via wicking and separating liquid/bubble pathway

Wicking is one of major phenomena on the nanostructured surfaces that explains the CHF enhancement by supplying liquid to local dry regions. Local dry spots were quenched by the dynamic liquid propagation on the wicking area. Therefore, the CHF improved due to the delay in vapor film formation caused by the decrease in SHPO area fraction, i.e., the increase in the wicking area. In prior research, to compare the micro-evaporated liquid supply abilities, the volumetric wicking rate was evaluated on nanostructured surfaces [61]. Here, we suggest the effective volumetric wicking rate ($W_{eff,V}$) which considers not only wicking abilities but also the effective wicking area fraction (A_{wick}/A_{total}) of the SBPI surface. The wicking area (A_{wick}) and effective volumetric wicking rate are defined as follows:

$$A_{wick} \equiv \text{total area} - \text{SHPO dot area} = p^2 - \pi d^2/4 \tag{5}$$

$$W_{eff,V} = (A_{wick}/A_{total})W^2(1-\varphi)h \tag{6}$$

where, W is the wicking rate. Fig. 9(a) demonstrates the CHF in relation to the effective volumetric wicking rate. SBPI_d0.5 and SBPI_d1.0 have lower effective volumetric wicking rate than the H-SHPI surface; thus, the CHF decreases via reduced micro scale liquid supply. However, CHF values have large difference on the Si plain and H-SHPO which have no wicking. Furthermore, the SBPI_d0.1 surface exhibited a greater CHF enhancement than the H-SHPI surface, which has a homogeneous superhydrophilicity and larger wicking area. These results imply that the wicking ability does not fully explain the CHF enhancement on the SBPI surfaces. Wicking is a micro scale liquid supply mechanism based on capillary pressure. In contrast, macro scale liquid supply to the heated area is another mechanism to prevent vapor film formation. Consequently, effective separation of the counterflow between downward liquid supply and upward bubble departure direction is another key factor in enhancing CHF.

During nucleation boiling, artificially dividing liquid supply and bubble departure path by surface modification secures a larger macro scale liquid supply to the boiling surface [69–71]. Previous research has shown that CHF has the highest value when the bubble departure diameter to bubble pitch ratio remains constant at 1 [32,49]. Therefore, we propose the dimensionless liquid supply factor (F_l) that incorporates both macro and micro scale liquid supply through bubble behaviors and wicking.

$$F_l = EXP\left[\frac{q''_{add,\ wick}}{q''_{CHF,\ plain}} - K\sqrt{\left(\frac{p}{D_b}-1\right)^2}\right] \tag{7}$$

where, $q''_{add,\ wick}$ is the additional heat dissipation caused by the evaporation of wicked liquid, $q''_{CHF,\ plain}$ is the CHF on the silicon plain surface, p is the pitch between nucleate sites, and D_b is the bubble departure diameter. K denotes the compensation value for fitting the linear relationship with CHF based on experimental results; it equals 0.1. $q''_{add,\ wick}$ is calculated as follow [18]:

$$q''_{add,\ wick} = \rho_l h_{lv} W_{eff,V} \Big/ \lambda_c^2 \tag{8}$$

where ρ_l is the density of liquid, h_{lv} is the latent heat of liquid-vapor phase, and λ_c is the critical wavelength. Fig. 9(b) shows the CHF enhancement of wettability control surfaces as the dimensionless liquid supply factor increases. Notably, only 0.26% of the effective volumetric wicking rate was reduced on the SBPI_d0.1 surface (i.e. 99.74% of wicking abilities were maintained) compared with H-SHPI surface; however, they have a larger advantage on macro scale liquid supply owing to separating the liquid and bubble pathway effectively. Hence, the CHF was improved by 100.4% and 12.2% compared to Si plain and with the SHPI surface, respectively. The experimental findings demonstrate that wicking and bubble behavior must be considered when analyzing liquid supply capabilities during pool boiling.

4. Conclusions

This study successfully demonstrated simultaneous enhancement of the HTC and CHF using the patterned SBPI surfaces with wicking. SBPI surfaces were strategically fabricated to achieve the hybrid effects of superhydrophobicity and superhydrophilicity. Local SHPO dots facilitated bubble nucleation and stabilized nucleate sites to boost HTC. The SHPI region, consisting of SiNWs, possessed both superhydrophilicity and dynamic wicking phenomena to further improve CHF via rapid liquid supply to the local dry region.

To evaluate HTC and CHF, pool boiling experiments were conducted on homogeneous wettability surfaces and SBPI surfaces. All SBPI surfaces increased the HTC regardless of SHPO area fractions due to

promoting nucleation and maximizing nucleate site density during pool boiling. The CHF was additionally enhanced on the SBPI_d0.1 surface compared to the H-SHPI surface, while other cases decreased the CHF. This result overcomes the pending issue of CHF reductions on the SBPI surface with wicking due to the suppression of dynamic liquid supply to SHPO regions.

Two significant CHF enhancement mechanisms and strategies were provided by evaluating the effective volumetric wicking rate and analyzing bubble departure characteristics. First, reducing SHPO area fractions maintained superhydrophilicity and wicking area for immediate micro scale liquid supply to dry spots. Second, macro scale liquid supply was secured by effectively separating liquid and bubble pathways to prevent developing into film boiling. Considering these two mechanisms, a dimensionless liquid supply factor was proposed and successfully utilized to verify the relationship to the CHF.

In conclusion, the pool boiling performance was enhanced by strategically controlling SBPI surfaces that have complex variables affecting boiling heat transfer. Employing multiscale techniques to enhance the liquid supply and bubble behaviors can further enhance boiling performance. SBPI surfaces with enhanced boiling performance can be utilized to effectively dissipate heat and prevent thermal failure in high-power generating systems.

CRediT authorship contribution statement

Dong Il Shim: Conceptualization, Methodology, Software, Validation, Investigation, Writing – original draft, Writing – review & editing. **Wei-Ting Hsu:** Investigation, Data curation, Validation, Writing – review & editing. **Maroosol Yun:** Investigation, Validation, Data curation. **Dongwhi Lee:** Investigation, Writing – review & editing. **Beom Seok Kim:** Investigation, Writing – review & editing. **Hyung Hee Cho:** Supervision, Conceptualization, Formal analysis, Project administration.

Declaration of Competing Interest

The authors declare that they have no known competing financial interests or personal relationships that could have appeared to influence the work reported in this paper.

Data availability

Data will be made available on request.

Acknowledgement

This work was supported by the Human Resources Development program (No.20204030200110) of the Korea Institute of Energy Technology Evaluation and Planning (KETEP) grant funded by the Korea government Ministry of Trade, Industry and Energy.

Supplementary materials

Supplementary material associated with this article can be found, in the online version, at doi:10.1016/j.ijmecsci.2023.108280.

References

[1] Mahmoud MM, Karayiannis TG. Pool boiling review: part I–Fundamentals of boiling and relation to surface design. Therm Sci Eng Prog 2021;25:101024. https://doi.org/10.1016/j.tsep.2021.101024.
[2] Sun Y, Tang Y, Zhang S, Yuan W, Tang H. A review on fabrication and pool boiling enhancement of three-dimensional complex structures. Renew Sust Energ Rev 2022;162:112437. https://doi.org/10.1016/j.rser.2022.112437.
[3] Cho HJ, Preston DJ, Zhu Y, Wang EN. Nanoengineered materials for liquid–vapour phase-change heat transfer. Nat Rev Mater 2017;2:16092. https://doi.org/10.1038/natrevmats.2016.92.
[4] Liang G, Mudawar I. Review of nanoscale boiling enhancement techniques and proposed systematic testing strategy to ensure cooling reliability and repeatability. Appl Therm Eng 2021;184:115982. https://doi.org/10.1016/j.applthermaleng.2020.1159.
[5] Mudawar I. Recent advances in high-flux, two-phase thermal management. J. Therm Sci Eng Appl 2013;5:021012. https://doi.org/10.1115/1.4023599.
[6] Suzuki K, Yuki K, Mochizuki M. Application of boiling heat transfer to high-heat-flux cooling technology in power electronics. Trans Jpn Inst Electron Packag 2011;4:127–33. https://doi.org/10.5104/jiepeng.4.127.
[7] Ali AF, El-Genk MS. Spreaders for immersion nucleate boiling cooling of a computer chip with a central hot spot. Energy Conv Manag 2012;53:259–67. https://doi.org/10.1016/j.enconman.2011.09.007.
[8] Moghadasi H, Saffari H. Experimental study of nucleate pool boiling heat transfer improvement utilizing micro/nanoparticles porous coating on copper surfaces. Int J Mech Sci 2021;196:106270. https://doi.org/10.1016/j.ijmecsci.2021.106270.
[9] Luo J, Wu S-Y, Xiao L, Zhou S-Y, Chen Z-L. Transient boiling heat transfer mechanism of droplet impacting heated cylinder. Int J Mech Sci 2022;233:107675. https://doi.org/10.1016/j.ijmecsci.2022.107675.
[10] Mehdikhani A, Moghadasi H, Saffari H. An experimental investigation of pool boiling augmentation using four-step electrodeposited micro/nanostructured porous surface in distilled water. Int J Mech Sci 2020;187:105924. https://doi.org/10.1016/j.ijmecsci.2020.105924.
[11] Liang G, Mudawar I. Review of pool boiling enhancement by surface modification. Int J Heat Mass Transf 2019;128:892–933. https://doi.org/10.1016/j.ijheatmasstransfer.2018.09.026.
[12] Song Y, Díaz-Marín CD, Zhang L, Cha H, Zhao Y, Wang EN. Three-tier hierarchical structures for extreme pool boiling heat transfer performance. Adv Mater 2022;34:2200899. https://doi.org/10.1002/adma.202200899.
[13] Jothi Prakash CG, Prasanth R. Enhanced boiling heat transfer by nano structured surfaces and nanofluids. Renew Sust Energ Rev 2018;82:4028–43. https://doi.org/10.1016/j.rser.2017.10.069.
[14] Zupančič M, Može M, Gregorčič P, Golobič I. Nanosecond laser texturing of uniformly and non-uniformly wettable micro structured metal surfaces for enhanced boiling heat transfer. Appl Surf Sci 2017;399:480–90. https://doi.org/10.1016/j.apsusc.2016.12.120.
[15] Mori S, Utaka Y. Critical heat flux enhancement by surface modification in a saturated pool boiling: a review. Int J Heat Mass Trasf 2017;108:2534–57. https://doi.org/10.1016/j.ijheatmasstransfer.2017.01.090.
[16] McCarthy M, Gerasopoulos K, Maroo SC, Hart AJ. Materials, fabrication, and manufacturing of micro/nano-structured surfaces for phase-change heat transfer enhancement. Nanoscale Microscale Thermophys Eng 2014;18:288–310. https://doi.org/10.1080/15567265.2014.926436.
[17] Ahn HS, Jo HJ, Kang SH, Kim MH. Effect of liquid spreading due to nano/microstructures on the critical heat flux during pool boiling. Appl Phys Lett 2011;98:071908. https://doi.org/10.1063/1.3555430.
[18] Kim BS, Lee H, Shin S, Choi G, Cho HH. Interfacial wicking dynamics and its impact on critical heat flux of boiling heat transfer. Appl Phys Lett 2014;105:191601. https://doi.org/10.1063/1.4901569.
[19] Rahman MM, Ölçeroğlu E, McCarthy M. Role of wickability on the critical heat flux of structured superhydrophilic surfaces. Langmuir 2014;30:11225–34. https://doi.org/10.1021/la5030923.
[20] Song Y, Wang C, Preston DJ, Su G, Rahman MM, Cha H, Seong JH, Philips B, Bucci M, Wang EN. Enhancement of boiling with scalable sandblasted surfaces. ACS Appl Mater Interfaces 2022;14:9788–94. https://doi.org/10.1021/acsami.1c22207.
[21] Haramura Y, Katto Y. A new hydrodynamic model of critical heat flux, applicable widely to both pool and forced convection boiling on submerged bodies in saturated liquids. Int J Heat Mass Tranf 1983;26:389–99. https://doi.org/10.1016/0017-9310(83)90043-1.
[22] Lienhard JH, Dhir VK. Hydrodynamic prediction of peak pool-boiling heat fluxes from finite bodies. J Heat Transf 1973;95:152–8. https://doi.org/10.1115/1.3450013.
[23] Rajvanshi A, Saini J, Prakash R. Investigation of macrolayer thickness in nucleate pool boiling at high heat flux. Int J Heat Mass Transf 1992;35:343–50. https://doi.org/10.1016/0017-9310(92)90272-T.
[24] Kandlikar SG. A theoretical model to predict pool boiling CHF incorporating effects of contact angle and orientation. J Heat Transfer 2001;123:1071–9. https://doi.org/10.1115/1.1409265.
[25] Chu K-H, Enright R, Wang EN. Structured surfaces for enhanced pool boiling heat transfer. Appl Phys Lett 2012;100:241603. https://doi.org/10.1063/1.4724190.
[26] Li R, Huang Z. A new CHF model for enhanced pool boiling heat transfer on surfaces with micro-scale roughness. Int J Heat Mass Transf 2017;109:1084–93.
[27] Mohanty RL, Das MK. A critical review on bubble dynamics parameters influencing boiling heat transfer. Renew Sust Energ Rev 2017;78:466–94. https://doi.org/10.1016/j.rser.2017.04.092.
[28] Wen R, Li Q, Wang W, Latour B, Li CH, Li C, Lee Y-C, Yang R. Enhanced bubble nucleation and liquid rewetting for highly efficient boiling heat transfer on two-level hierarchical surfaces with patterned copper nanowire arrays. Nano Energy 2017;38:59–65. https://doi.org/10.1016/j.nanoen.2017.05.028.
[29] Heidary A, Moghadasi H, Saffari H. Impact of dimensional characteristics of low-conductive channels on the enhancement of pool boiling: an experimental analysis. Int J Mech Sci 2021;209:106710. https://doi.org/10.1016/j.ijmecsci.2021.106710.
[30] Liu Y, Lu MC, Xu D. The suppression effect of easy-to-activate nucleation sites on the critical heat flux in pool boiling. Int J Therm Sci 2018;129:231–7. https://doi.org/10.1016/j.ijthermalsci.2018.03.007.

[31] Pi G, Deng D, Chen L, Xu X, Zhao C. Pool boiling performance of 3D-printed reentrant microchannels structures. Int J Heat Mass Transf 2020;156:119920. https://doi.org/10.1016/j.ijheatmasstransfer.2020.119920.
[32] Lee D, Lee N, Shim DI, Kim BS, Cho HH. Enhancing thermal stability and uniformity in boiling heat transfer using micro-nano hybrid surfaces (MNHS). Appl Therm Eng 2018;130:710–21. https://doi.org/10.1016/j.applthermaleng.2017.10.144.
[33] Kim DE, Yu DI, Jerng DW, Kim MH, Ahn HS. Review of boiling heat transfer enhancement on micro/nanostructured surfaces. Exp Therm Fluid Sci 2015;66:173–96. https://doi.org/10.1016/j.expthermflusci.2015.03.023.
[34] Bai L, Zhang L, Lin G, Peterson GP. Pool boiling with high heat flux enabled by a porous artery structure. Appl Phys Lett 2016;108:233901. https://doi.org/10.1063/1.4953574.
[35] Ha M, Graham S. Pool boiling characteristics and critical heat flux mechanisms of microporous surfaces and enhancement through structural modification. Appl Phys Lett 2017;111:091601. https://doi.org/10.1063/1.4999158.
[36] Mori S, Maruoka N, Okuyama K. Critical heat flux enhancement by a two-layer structured honeycomb porous plate in a saturated pool boiling of water. Int J Heat Mass Transf 2018;118:429–38. https://doi.org/10.1016/j.ijheatmasstransfer.2017.10.100.
[37] Liu H, Zhang C, Wang J, Zhang L. Critical heat flux enhancement using composite porous structure produced by selective laser melting. Appl Therm Eng 2021;197:117396. https://doi.org/10.1016/j.applthermaleng.2021.117396.
[38] Elkholy A, Kempers R. Enhancement of pool boiling heat transfer using 3D-printed polymer fixtures. Exp Therm Fluid Sci 2020;114:110056. https://doi.org/10.1016/j.expthermflusci.2020.110056.
[39] Betz AR, Xu J, Qiu H, Attinger D. Do surfaces with mixed hydrophilic and hydrophobic areas enhance pool boiling? Appl Phys Lett 2010;97:141909. https://doi.org/10.1063/1.3485057.
[40] Jo HJ, Ahn HS, Kang SH, Kim MH. A study of nucleate boiling heat transfer on hydrophilic, hydrophobic and heterogeneous wetting surfaces. Int J Heat Mass Transf 2011;54:5643–52. https://doi.org/10.1016/j.ijheatmasstransfer.2011.06.001.
[41] Jo HJ, Kim SH, Park HS, Kim MW. Critical heat flux and nucleate boiling on several heterogeneous wetting surfaces: controlled hydrophobic patterns on a hydrophilic substrate. Int J Multiph Flow 2014;62:101–9. https://doi.org/10.1016/j.ijmultiphaseflow.2014.02.006.
[42] Shen B, Yamada M, Hidaka S, Liu J, Shiomi J, Amberg G, Do-Quang M, Kohno M, Takahashi K, Takata Y. Early onset of nucleate boiling on gas-covered biphilic surfaces. Sci Rep 2017;7:2036. https://doi.org/10.1038/s41598-017-02163-8.
[43] Hsu W-T, Lee D, Lee N, Yun M, Cho HH. Enhancement of flow boiling heat transfer using heterogeneous wettability patterned surfaces with varying inter-spacing. Int J Heat Mass Transf 2021;164:120596. https://doi.org/10.1016/j.ijheatmasstransfer.2020.120596.
[44] Zhang W, Chai Y, Xu J, Liu G, Sun Y. 3D heterogeneous wetting microchannel surfaces for boiling heat transfer enhancement. Appl Surf Sci 2018;457:891–901. https://doi.org/10.1016/j.apsusc.2018.07.021.
[45] Ateş A, Benam BP, Mohammadilooey M, Çelik S, Serdyukov V, Surtaev A, Sadaghiani AK, Koşar A. superhydrophobic, superhydrophilic, and superbiphilic surfaces at atmospheric and sub-atmospheric pressures. Int J Heat Mass Transf 2023;201:123582. https://doi.org/10.1016/j.ijheatmasstransfer.2022.123582.
[46] Motezakker AR, Sadaghiani AK, Celik S, Larsen T, Villanueva LG, Koşar A. Optimum ratio of hydrophobic to hydrophilic areas of biphilic surfaces in thermal fluid systems involving boiling. Int J Heat Mass Transf 2019;135:164–74. https://doi.org/10.1016/j.ijheatmasstransfer.2019.01.139.
[47] Sujith Kumar CS, Chang YW, Chen P-H. Effect of heterogeneous wettable structures on pool boiling performance of cylindrical copper surfaces. Appl Therm Eng 2017;127:1184–93. https://doi.org/10.1016/j.applthermaleng.2017.08.069.
[48] Liang G, Chen Y, Wang J, Wang Z, Shen S. Experiments and modeling of boiling heat transfer on hybrid-wettability surfaces. Int J Multiph Flow 2021;144:103810. https://doi.org/10.1016/j.ijmultiphaseflow.2021.103810.
[49] Može M, Zupančič M, Golobič I. Pattern geometry optimization on superbiphilic aluminum surfaces for enhanced pool boiling heat transfer. Int J Heat Mass Transf 2020;161:120265. https://doi.org/10.1016/j.ijheatmasstransfer.2020.120265.
[50] Jo HJ, Park HS, Kim MH. Single bubble dynamics on hydrophobic–hydrophilic mixed surfaces. Int J Heat Mass Transf 2016;93:554–65. https://doi.org/10.1016/j.ijheatmasstransfer.2015.09.031.
[51] Lim DY, Bang IC. Controlled bubble departure diameter on biphilic surfaces for enhanced pool boiling heat transfer performance. Int J Heat Mass Transf 2020;150:119360. https://doi.org/10.1016/j.ijheatmasstransfer.2020.119360.
[52] Betz AR, Jenkins J, Attinger D. Boiling heat transfer on superhydrophilic, superhydrophobic, and superbiphilic surfaces. Int J Heat Mass Transf 2013;57:733–41. https://doi.org/10.1016/j.ijheatmasstransfer.2012.10.080.
[53] Rahman MM, McCarthy M. Boiling enhancement on nanostructured surfaces with engineered variations in wettability and thermal conductivity. Heat Transf Eng 2017;38:1285–95. https://doi.org/10.1080/01457632.2016.1242961.
[54] Huang Z, Geyer N, Werner P, de Boor J, Gosele U. Metal-assisted chemical etching of silicon: a review. Adv Mater 2011;23:285–308. https://doi.org/10.1002/adma.201001784.
[55] Wenzel RN. Resistance of solid surfaces to wetting by water. Ind Eng Chem 1936;28:988–94. https://doi.org/10.1021/ie50320a024.
[56] Kim BS, Shin S, Shin SJ, Kim KM, Cho HH. Control of superhydrophilicity/superhydrophobicity using silicon nanowires via electroless etching method and fluorine carbon coatings. Langmuir 2011;27:10148–56. https://doi.org/10.1021/la200940j.
[57] Cassie ABD, Baxter S. Wettability of porous surfaces. Trans Faraday Soc 1944;40:546–51. https://doi.org/10.1039/tf9444000546.
[58] Wang X, Ding B, Yu J, Wang M. Engineering biomimetic superhydrophobic surfaces of electrospun nanomaterials. Nano Today 2011;6:510–30. https://doi.org/10.1016/j.nantod.2011.08.004.
[59] Lee SH, Kang BS, Kwak MK. Facile design and realization of extremely water-repellent surface by mimicking the greta oto's wings. Int J Mech Sci 2022;222:107218. https://doi.org/10.1016/j.ijmecsci.2022.107218.
[60] Kim BS, Choi G, Shim DI, Kim KM, Cho HH. Surface roughening for hemi-wicking and its impact on convective boiling heat transfer. Int J Heat Mass Transf 2016;102:1100–7. https://doi.org/10.1016/j.ijheatmasstransfer.2016.07.008.
[61] Shim DI, Choi G, Lee N, Kim T, Kim BS, Cho HH. Enhancement of pool boiling heat transfer using aligned silicon nanowire arrays. ACS Appl Mater Interfaces 2017;9:17595–602. https://doi.org/10.1021/acsami.7b01929.
[62] Liu X, Zhang J, Hu X, Wu D. Influence of tool material and geometry on micro-textured surface in radial ultrasonic vibration-assisted turning. Int J Mech Sci 2019;152:545–57. https://doi.org/10.1016/j.ijmecsci.2019.01.027.
[63] Misyura SY. Dependence of wettability of microtextured wall on the heat and mass transfer: simple estimates for convection and heat transfer. Int J Mech Sci 2020;170:105353. https://doi.org/10.1016/j.ijmecsci.2019.105353.
[64] Samanta A, Wang Q, Shaw SK, Ding H. Roles of chemistry modification for laser textured metal alloys to achieve extreme surface wetting behaviors. Mater Des 2020;192:108744. https://doi.org/10.1016/j.matdes.2020.108744.
[65] Moffat RJ. Describing the uncertainties in experimental results. Exp Therm Fluid Sci 1988;1:3–17. https://doi.org/10.1016/0894-1777(88)90043-X.
[66] Song Y, Zhang L, Díaz-Marín CD, Cruz SS, Wang EN. Unified descriptor for enhanced critical heat flux during pool boiling of hemi-wicking surfaces. Int J Heat Mass Transf 2022;183:122189. https://doi.org/10.1016/j.ijheatmasstransfer.2021.122189.
[67] Chen R, Lu M-C, Srinivasan V, Wang Z, Cho HH, Majumdar A. Nanowires for enhanced boiling heat transfer. Nano Lett 2009;9:548–53. https://doi.org/10.1021/nl8026857.
[68] Kim BS, Shin S, Lee D, Choi G, Lee H, Kim KM, Cho HH. Stable and uniform heat dissipation by nucleate-catalytic nanowires for boiling heat transfer. Int J Heat Mass Transf 2014;70:23–32. https://doi.org/10.1016/j.ijheatmasstransfer.2013.10.061.
[69] Kandlikar SG. Enhanced macroconvection mechanism with separate liquid–vapor pathways to improve pool boiling performance. J Heat Transf 2017;139:051501. https://doi.org/10.1115/1.4035247.
[70] Jaikumar A, Kandlikar SG. Pool boiling enhancement through bubble induced convective liquid flow in feeder microchannels. Appl Phys Lett 2016;108:041604. https://doi.org/10.1063/1.4941032.
[71] Mahmoud MM, Karayiannis TG. Pool boiling review: part II–Heat transfer enhancement. Therm Sci Eng Prog 2021;25:101023. https://doi.org/10.1016/j.tsep.2021.101023.